Electric Power Systems Research 80 (2010) 514–527

Contents lists available at ScienceDirect

Electric Power Systems Research

journal homepage: www.elsevier.com/locate/epsr

Sliding mode based load-frequency control in power systems

K. Vrdoljak*, N. Perić, I. Petrović

University of Zagreb, Faculty of Electrical Engineering and Computing, 10000 Zagreb, Croatia

ARTICLE INFO

Article history:
Received 17 April 2008
Received in revised form 28 July 2009
Accepted 24 October 2009
Available online 24 November 2009

Keywords:
Sliding mode control
Load-frequency control
Fast output sampling
Genetic algorithm
Uncertainties

ABSTRACT

The paper presents a new discrete-time sliding mode controller for load-frequency control (LFC) in control areas (CAs) of a power system. As it uses full-state feedback it can be applied for LFC not only in CAs with thermal power plants but also in CAs with hydro power plants, in spite of their non-minimum phase behaviors. To enable full-state feedback we have proposed a state estimation method based on fast sampling of measured output variables, which are frequency, active power flow interchange and generated power from power plants engaged in LFC in the CA. The same estimation method is also used for the estimation of external disturbances in the CA, what additionally improves the overall system behavior. Design of the discrete-time sliding mode controller for LFC with desired behavior is accomplished by using a genetic algorithm. To the best of our knowledge, proposed controller outperforms any of the existing controllers in fulfilling the requirements of LFC. It was thoroughly compared to the commonly used PI controller by extensive simulation experiments on a power system with four interconnected CAs. These experiments show that the proposed controller ensures better disturbance rejection, maintains required control quality in the wider operating range, shortens the frequency's transient response avoiding the overshoot and is more robust to uncertainties in the system.

1. Introduction

Power systems are composed of interconnected subsystems or control areas (CAs). Most of European countries are members of "Union for the Co-ordination of Transmission of Electricity" (UCTE) interconnection [1]. It is assumed that each CA consists of a coherent group of generators. CAs are interconnected by the tie-lines. Because of the differences in generation and load in a power system, system's frequency deviates from its nominal value and active power flow interchanges between areas deviate from their contracted values. The purpose of load-frequency control (LFC) in each CA is to compensate for those deviations. That is obtained by changing power outputs of certain generators within the CA. To test LFC algorithms, an example power system is usually modeled as an interconnection of a few CAs. Since all generators in one CA are coherent, all power plants engaged in LFC in a CA can be replaced with one substitute power plant [2]. In some CAs that power plant is of thermal type and in some CAs of hydro type. When modeling a CA, power imbalance and losses can be seen as external disturbances.

Nowadays, in the majority of CAs PI type controllers with constant parameters are used for LFC [3–6]. However, systems with PI control have long settling time and relatively large overshoots in frequency's transient responses [7]. Besides, PI control algorithm provides required behavior of the system only in the vicinity of the nominal operating point, for which it is designed. But, operating point of a power system usually changes a lot, which is primarily caused by the amount and characteristic of power consumption, characteristics of power plants and the number of power plants engaged in LFC in a CA. Future power systems will rely on large amounts of distributed generation with large percentage of renewable energy based sources, what will further increase system uncertainties and thereby induce new requirements to the LFC system [8]. The shortening of time periods in which each level of frequency regulation must finish could be also expected in the future [9].

Therefore, an advanced controller should be developed and used instead of the PI controller in order to: (1) ensure better disturbance rejection, (2) maintain required control quality in the wider operating range, (3) shorten the frequency's transient responses avoiding the overshoots and (4) be robust to uncertainties in the system. Additionally, a new control algorithm for a CA should enable decentralized LFC of interconnected CAs, i.e. its structure and parameters must not depend on applied controllers in neighboring CAs. It should also be a discrete-time control algorithm with sampling time in the range 1–5 s as required in UCTE interconnection [1]. Finally, it should be relatively simple to implement,

* Corresponding author at: University of Zagreb, Faculty of Electrical Engineering and Computing, Department of Control and Computer Engineering, Unska 3, 10000 Zagreb, Croatia. Tel: +385 1 6129 795; fax: +385 1 6129 809.
E-mail addresses: kresimir.vrdoljak@fer.hr (K. Vrdoljak), nedjeljko.peric@fer.hr (N. Perić), ivan.petrovic@fer.hr (I. Petrović).

0378-7796/$ – see front matter © 2009 Elsevier B.V. All rights reserved.
doi:10.1016/j.epsr.2009.10.026

in order to be accepted as adequate replacement of PI control algorithm.

Recently, many different control algorithms have been proposed for LFC [10,11] in order to overcome limitations of the PI controller. Among them, the most immanent are based on: robust control, [5,12], fuzzy logic [13–15], neural networks [16–18], model predictive control [19,20], optimal control [21–23], adaptive control [24–26] and sliding mode control (SMC) [27–31] algorithms. Some drawbacks present in the above algorithms can be listed as follows: (1) measurements from neighbor CAs are required for controller synthesis, but obtaining them could be impractical in real power system [25,27]; (2) control signal is computed in continuous-time [5,15,27–32] although in real power system the signal should be sent to the power plants in discrete-time; (3) controllers are based on full system state, but with no estimator present [14,22,27–31]; (4) controllers are complex and of high order [20]; (5) there is a requirement for on-line parameters identification [24,30]; (6) the choosing of appropriate controller parameters is problematic [23,29,32]. Listed drawbacks clearly indicate that none of the abovementioned controllers fulfills all requirements for LFC.

In this paper we propose a discrete-time sliding mode controller that at best of our knowledge outperforms any of the existing controllers in fulfilling the requirements for LFC. Generally, SMC is a robust control technique that shows very good behavior in controlling systems with external disturbances and parameter variations [33]. In SMC, system closed-loop behavior is determined by a submanifold in the state space, which is called a sliding surface. The goal of the sliding mode control is to drive the system trajectory to reach the sliding surface and then to stay on it. When the trajectory is on the surface, system invariance to particular uncertainties and parameter variations is guaranteed.

Ideal sliding of the system trajectory along the sliding surface can be achieved only by the continuous-time SMC with very high (theoretically infinite) switching frequency of the control signal. But, real power plants are unable to respond to so fast changes of the control signal, and that is the reason why we propose a discrete-time sliding mode controller which changes control signal periodically in discrete-time instants. Of course, with the usage of discrete-time SMC the system trajectory can't be kept on the sliding surface but inside a small band around the surface. That behavior is known as quasi sliding mode [34]. Two main problems in designing discrete-time SMC for LFC are appropriate choices of sliding surface which defines desired system behavior, and of reaching law which must be chosen to ensure convergence of the trajectory from any point in the state space towards the surface [35]. An optimization method based on genetic algorithm (GA) is proposed for finding optimal parameters of the sliding surface and of the reaching law.

If only thermal power plants are used for LFC in a CA then stable sliding mode controller can be also designed using only measured output signals, which are frequency, active power flow interchange and generated power from each power plant in that CA. But, if hydro power plants are used for LFC then full-state feedback is needed because of their non-minimum phase behaviors. We have developed a full-state sliding mode controller, which can be applied in either cases. The usage of the state estimation method based on fast output sampling (FOS) [36] is proposed, what is possible due to availability of multiple measurements of output signals in each sampling period of the controller. FOS estimation method is also used for the estimation of external disturbances, what additionally improves the overall system behavior.

The brief outline of the paper is as follows: Section 2 presents power system model, Section 3 describes state and disturbance estimation technique. Section 4 gives an overview of discrete-time SMC and its application to LFC. Section 5 presents a GA used for the purpose of finding optimal sliding mode algorithm parameters, while Section 6 contains simulation results.

2. Mathematical model of a power system

An example mathematical model of a power system used in this paper consists of four interconnected CAs, each represented with one substitute thermal or hydro power plant. Each CA has its own load frequency controller, as it is shown in Fig. 1. Power system is modeled as continuous, while control signals are sent to the plants in discrete-time.

It is supposed that power plants in CA1 and CA4 are thermal power plants, while power plants in CA2 and CA3 are hydro power plants. Furthermore, power plants in CA1 and CA2 have less generating capacity then those in CA3 and CA4. Sliding mode based LFC, described in Section 4, will be applied to CA1 and CA3, while LFC in other CAs will be based on conventional PI type control algorithm.

Linearized mathematical model of each of four CAs can be described with the following equation:

$$\dot{\mathbf{x}}_i(t) = \mathbf{A}_i\mathbf{x}_i(t) + \sum_j \mathbf{A}_{ij}\mathbf{x}_j(t) + \mathbf{B}_i\mathbf{u}_i(t) + \mathbf{F}_i\mathbf{d}_i(t) + \boldsymbol{\xi}_i(\mathbf{x}, \mathbf{u}, t), \quad (1)$$

where $\mathbf{x}_i \in \mathbb{R}^n$ is the system state vector, $\mathbf{x}_j \in \mathbb{R}^p$ is a state vector of the neighbor system, $\mathbf{u}_i \in \mathbb{R}^m$ is the control signal vector, $\mathbf{d}_i \in \mathbb{R}^k$ is the disturbance vector, $\boldsymbol{\xi}_i$ is a vector of uncertainties and $\mathbf{y} \in \mathbb{R}^l$ is the output vector. Matrices in (1) have appropriate dimensions: $\mathbf{A}_i \in \mathbb{R}^{n\times n}$, $\mathbf{A}_{ij} \in \mathbb{R}^{n\times p}$, $\mathbf{B}_i \in \mathbb{R}^{n\times m}$, $\mathbf{F}_i \in \mathbb{R}^{n\times k}$ and $\mathbf{C}_i \in \mathbb{R}^{l\times n}$.

Linearized model of CAs are used instead of the nonlinear ones because proposed SMC is based on such a linear model, where linearization error is included in the uncertainty term $\boldsymbol{\xi}_i(\mathbf{x}, \mathbf{u}, t)$. Simplified linearized continuous-time models of CAs with one substitute hydro or thermal power plant are shown in Figs. 2 and 3, respectively.

For the model shown in Fig. 2 state and disturbance vectors from (1) are (see Table 1):

$$\mathbf{x}_i(t) = \begin{bmatrix} \Delta f_i(t) \\ \Delta P_{tiei}(t) \\ \Delta P_{gi}(t) \\ \Delta x_{gi}(t) \\ \Delta x_{ghi}(t) \end{bmatrix}, \mathbf{d}_i(t) = \Delta P_{di}(t). \quad (2)$$

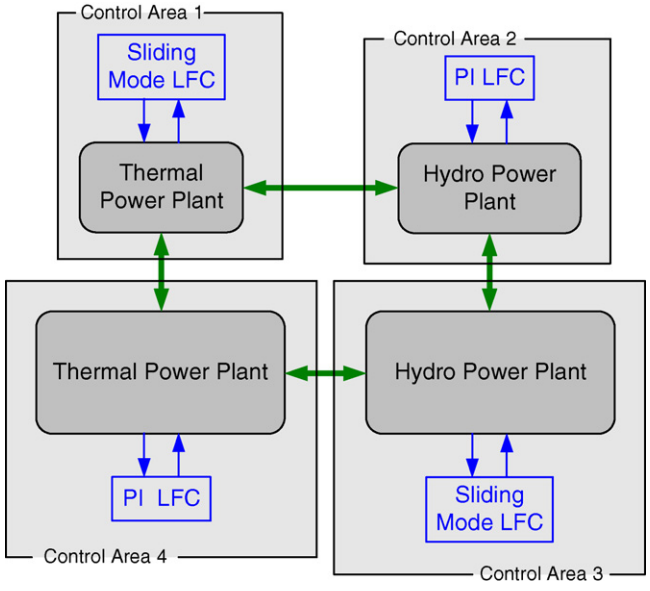

Fig. 1. Four interconnected control areas.

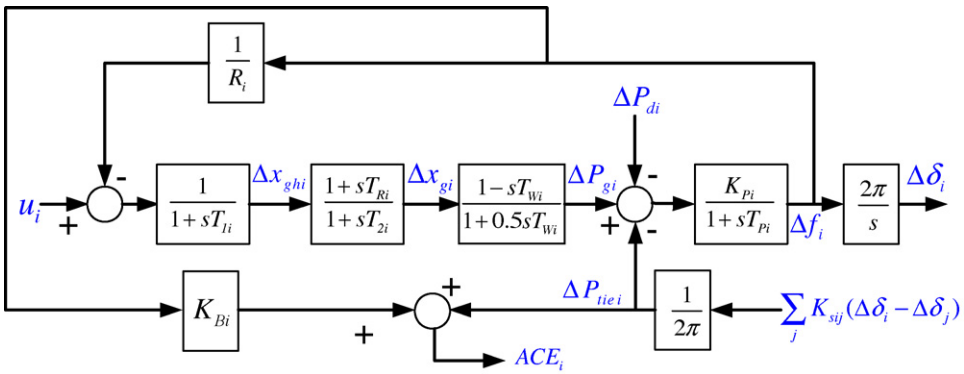

Fig. 2. The block diagram of i-th control area represented with hydro power plant.

Matrices in (1) are:

$$\mathbf{A}_i = \begin{bmatrix} -\frac{1}{T_{Pi}} & -\frac{K_{Pi}}{T_{Pi}} & \frac{K_{Pi}}{T_{Pi}} & 0 & 0 \\ \sum_j K_{Sij} & 0 & 0 & 0 & 0 \\ 2\alpha & 0 & -\frac{2}{T_{Wi}} & 2\gamma & 2\beta \\ -\alpha & 0 & 0 & -\frac{1}{T_{2i}} & -\beta \\ -\frac{1}{T_{1i}R_i} & 0 & 0 & 0 & -\frac{1}{T_{1i}} \end{bmatrix},$$

$$\mathbf{B}_i = \begin{bmatrix} 0 \\ 0 \\ -2R_i\beta \\ R_i\beta \\ \frac{1}{T_{1i}} \end{bmatrix}, \mathbf{F}_i = \begin{bmatrix} -\frac{K_{Pi}}{T_{Pi}} \\ 0 \\ 0 \\ 0 \\ 0 \end{bmatrix}, \tag{3}$$

with coefficients:

$$\alpha = \frac{T_{Ri}}{T_{1i}T_{2i}R_i}, \beta = \frac{T_{Ri}-T_{1i}}{T_{1i}T_{2i}}, \gamma = \frac{T_{2i}+T_{Wi}}{T_{2i}T_{Wi}}. \tag{4}$$

Matrices $\mathbf{A}_{ij}$ in (1) have dimensions 5×4 or 5×5, depending on whether they are used to describe hydro–thermal or hydro–hydro connection. All of their elements are equal to zero, except the element at position $(1, 2)$, which is equal to $-K_{Sij}$.

For the model shown in Fig. 3 state and disturbance vectors from (1) are:

$$\mathbf{x}_i(t) = \begin{bmatrix} \Delta f_i(t) \\ \Delta P_{tiei}(t) \\ \Delta P_{gi}(t) \\ \Delta x_{gi}(t) \end{bmatrix}, \mathbf{d}_i(t) = \Delta P_{di}(t), \tag{5}$$

while matrices in (1) are:

$$\mathbf{A}_i = \begin{bmatrix} -\frac{1}{T_{Pi}} & -\frac{K_{Pi}}{T_{Pi}} & \frac{K_{Pi}}{T_{Pi}} & 0 \\ \sum_j K_{Sij} & 0 & 0 & 0 \\ 0 & 0 & -\frac{1}{T_{Ti}} & \frac{1}{T_{Ti}} \\ -\frac{1}{T_{Gi}R_i} & 0 & 0 & -\frac{1}{T_{Gi}} \end{bmatrix},$$

$$\mathbf{B}_i = \begin{bmatrix} 0 \\ 0 \\ 0 \\ \frac{1}{T_{Gi}} \end{bmatrix}, \mathbf{F}_i = \begin{bmatrix} -\frac{K_{Pi}}{T_{Pi}} \\ 0 \\ 0 \\ 0 \end{bmatrix}. \tag{6}$$

In this case, matrices $\mathbf{A}_{ij}$ in (1) have dimensions 4×4 or 4×5, depending on whether they are used to describe thermal–thermal or thermal–hydro connection. Again, all of their elements are equal to zero, except the element at position $(1, 2)$, which is equal to $-K_{Sij}$.

Signals and parameters used in the models from Figs. 2 and 3 are shown in Table 1.

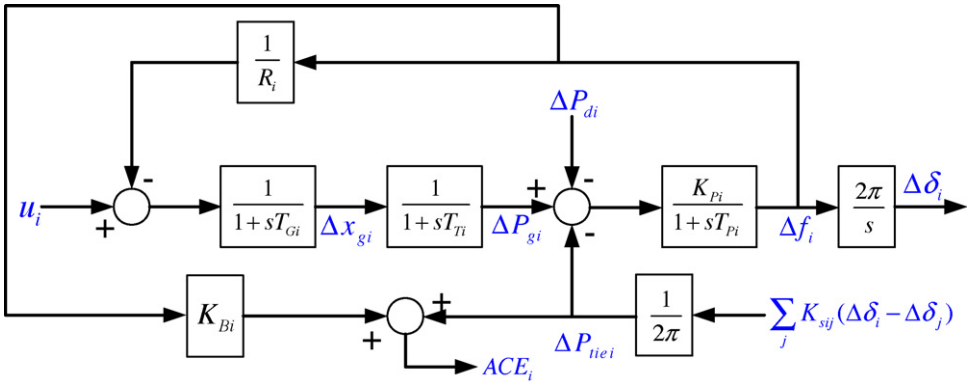

Fig. 3. The block diagram of i-th control area represented with thermal power plant.

Table 1
Power system variables and parameters.

Parameter/variable	Description	Unit
$\Delta f(t)$	Frequency deviation	Hz
$\Delta P_g(t)$	Generator output power deviation	p.u.MW
$\Delta x_g(t)$	Governor valve position deviation	p.u.
$\Delta x_{gh}(t)$	Governor valve servomotor position deviation	p.u.
$\Delta P_{tie}(t)$	Tie-line active power deviation	p.u.MW
$\Delta P_d(t)$	Load disturbance	p.u.MW
$\Delta\delta(t)$	Rotor angle deviation	rad
K_P	Power system gain	Hz / p.u.MW
T_P	Power system time constant	s
T_W	Water starting time	s
T_1, T_2, T_R	Hydro governor time constants	s
T_G	Thermal governor time constant	s
T_T	Turbine time constant	s
K_S	Interconnection gain between CAs	p.u.MW
K_B	Frequency bias factor	p.u.MW / Hz
R	Speed droop due to governor action	Hz / p.u.MW
ACE	Area control error	p.u.MW

UCTE prescribes a set of rules and recommendations about LFC for its members. Thereby, an area control error (ACE) signal is introduced as a quantitive measure of CA's deviation from the proposed behavior. ACE is defined as a combination of frequency deviation in a CA and of active power flow deviation in tie-lines connecting a CA with the neighbor areas. The goal of LFC in each area is to compensate for ACE deviations. Therefore, let the output of the system (1) be defined as:

$$\mathbf{y}_i(t) = \mathbf{C}_i\mathbf{x}_i(t) = ACE_i(t) = K_{Bi}\Delta f_i(t) + \Delta P_{tiei}(t), \tag{7}$$

where parameter K_B is tuned in a way that ensures ACE different than zero only for a CA in which the disturbance occurs. In all other CAs, values of ACE signals are not significantly affected by that disturbance.

Matrix $\mathbf{C}_i$ in (7) is $\mathbf{C}_i = [\,K_{Bi} \quad 1 \quad 0 \quad 0 \quad 0\,]$ for a CA with hydro power plant and $\mathbf{C}_i = [\,K_{Bi} \quad 1 \quad 0 \quad 0\,]$ for a CA with thermal power plant.

3. System state and disturbance estimation

A general continuous-time linear system with added disturbance and neglected uncertainties can be described with the following equations:

$$\begin{aligned}\dot{\mathbf{x}}(t) &= \mathbf{A}\mathbf{x}(t) + \mathbf{B}\mathbf{u}(t) + \mathbf{F}\mathbf{d}(t),\\ \mathbf{y}(t) &= \mathbf{C}\mathbf{x}(t).\end{aligned} \tag{8}$$

Let us assume that control signal $\mathbf{u}$ from (8) is able to change its value only every τ seconds, where τ is a sampling period.

In order to design discrete-time estimator, system (8) is discretized using the Zero-Order-Hold (ZOH) discretization method, with sampling period τ. That results in the following discrete-time system:

$$\begin{aligned}\mathbf{x}((k+1)\tau) &= \mathbf{G}_\tau\mathbf{x}(k\tau) + \mathbf{H}_\tau\mathbf{u}(k\tau) + \mathbf{W}_\tau\mathbf{d}(k\tau),\\ \mathbf{y}(k\tau) &= \mathbf{C}\mathbf{x}(k\tau).\end{aligned} \tag{9}$$

Matrices in (9) are defined as follows:

$$\begin{aligned}\mathbf{G}_\tau &= e^{\mathbf{A}\tau},\\ \mathbf{H}_\tau &= \int_0^\tau e^{\mathbf{A}t}\mathbf{B}dt,\\ \mathbf{W}_\tau &= \int_0^\tau e^{\mathbf{A}t}\mathbf{F}dt.\end{aligned} \tag{10}$$

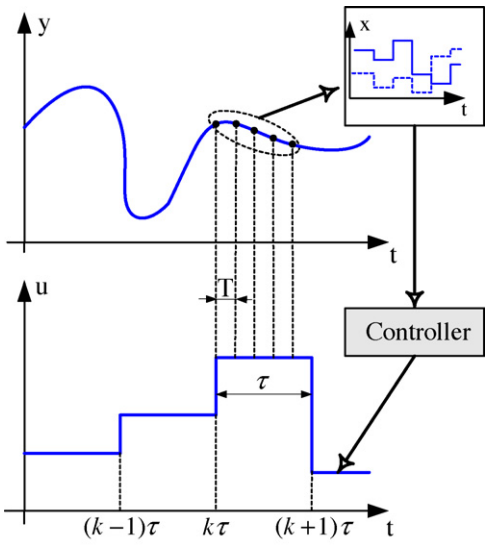

Fig. 4. The usage of the FOS estimation method in system control.

Let us also assume that only system output is measurable, and only at certain time instances, $\mathbf{y}(kT)$, where T is a subsampling period:

$$T = \frac{\tau}{N}, \tag{11}$$

where $N \in \mathbb{N}$. Those samples can be used as input signals of the appropriate estimator for unmeasured state and disturbance signals in (8).

LFC applied nowadays in real power systems is an example of a system with multiple sampling periods. In LFC, control signal is sent to the power plants in discrete-time. In UCTE interconnection that period is 1–5 s [6]. Additionally, during one sampling period several measurements of frequency $f(kT)$ and tie-line power $P_{tie}(kT)$ signals are gathered. Besides those subsamples, which are inputs to classical PI controller, subsamples of generated power $P_g(kT)$ are also gathered for monitoring purposes. Those samples could also be used as inputs to the estimator. Because a substitute power plant is used in modeling a CA and also in controller synthesis, all other state and disturbance signals, that cannot be measured in the real system, must therefore be estimated.

3.1. Fast output sampling method

Fast output sampling (FOS) is an estimation technique appropriate for continuous time system controlled with discrete-time control signal, where the output signal can be sampled several times during one period of the control signal [36]. FOS shows better performance than standard estimation techniques, because it reduces the estimation error to zero after just one sampling period [34]. Standard estimators need at least ν sampling periods to achieve errorless estimation, where ν is the observability index of the system [37]. To use FOS estimation technique, it must be satisfied $N \geq \nu$ [36].

The principle of using FOS estimation technique in system control is shown in Fig. 4. Firstly, the last N subsamples of the output signal $\mathbf{y}(t)$, measured in the most recent sampling period τ, are used to estimate the system state. Then, that estimated state is used to compute the control signal for the next sampling period.

Consider system (8), sampled at subsampling period T:

$$\begin{aligned}\mathbf{x}((k+1)T) &= \mathbf{G}_T\mathbf{x}(kT)+\mathbf{H}_T\mathbf{u}(kT)+\mathbf{W}_T\mathbf{d}(kT),\\ \mathbf{y}(kT) &= \mathbf{C}\mathbf{x}(kT).\end{aligned} \tag{12}$$

It should be noted that system (12) has different sampling period than system (9). Its matrices $\mathbf{G}_T$, $\mathbf{H}_T$ and $\mathbf{W}_T$ are defined similar to those in (10), just with subsampling period T instead of sampling period τ. Relation between those two sampling periods is given with (11).

System with fast output sampling can be described by combining (9) and (12). Generally, let the input vector of that system be decoupled into two components: $\mathbf{u}_\tau$ (with sampling period τ) and $\mathbf{u}_T$ (with subsampling period T).

The system's N consecutive subsamples, taken during the sampling period τ, can now be calculated as:

$$\begin{aligned}\mathbf{x}(k\tau+T) &= \mathbf{G}_T\mathbf{x}(k\tau)+\mathbf{H}_T(\mathbf{u}_\tau(k\tau)+\mathbf{u}_T(k\tau))\\ &\quad +\mathbf{W}_T\mathbf{d}(k\tau),\\ \mathbf{x}(k\tau+2T) &= \mathbf{G}_T^2\mathbf{x}(k\tau)+(\mathbf{G}_T\mathbf{H}_T+\mathbf{H}_T)\mathbf{u}_\tau(k\tau)\\ &\quad +\mathbf{G}_T\mathbf{H}_T\mathbf{u}_T(k\tau)+\mathbf{H}_T\mathbf{u}_T(k\tau+T)\\ &\quad +(\mathbf{G}_T\mathbf{W}_T+\mathbf{W}_T)d(k\tau),\\ &\vdots\\ \mathbf{x}(k\tau+(N-1)T) &= \mathbf{G}_T^{N-1}\mathbf{x}(k\tau)+\sum_{i=0}^{N-2}(\mathbf{G}_T^i\mathbf{H}_T)\mathbf{u}_\tau(k\tau)\\ &\quad +\mathbf{G}_T^{N-2}\mathbf{H}_T\mathbf{u}_T(k\tau)\\ &\quad +\mathbf{G}_T^{N-3}\mathbf{H}_T\mathbf{u}_T(k\tau+T)+\dots\\ &\quad +\mathbf{H}_T\mathbf{u}_T(k\tau+(N-2)T)\\ &\quad +\sum_{i=0}^{N-2}(\mathbf{G}_T^i\mathbf{W}_T)d(k\tau).\end{aligned} \tag{13}$$

It is assumed here that the disturbance $\mathbf{d}(k\tau)$ has a constant value during the whole sampling period τ. That assumption is reasonable for LFC because in real power systems changes of $\Delta P_d(t)$ during one sampling period τ can be neglected. It is also assumed that there is no direct influence of input signal to system's output, i.e. $\mathbf{D}=\mathbf{0}$.

A procedure to estimate unmeasured state and disturbance starts from a vector of output subsamples $\mathbf{y}_k^*$, which consists of the last N output subsamples, sampled in the most recent sampling period τ. It is:

$$\mathbf{y}_k^*=\begin{bmatrix}\mathbf{y}(k\tau)\\ \mathbf{y}(k\tau+T)\\ \mathbf{y}(k\tau+2T)\\ \vdots\\ \mathbf{y}(k\tau+(N-2)T)\\ \mathbf{y}(k\tau+(N-1)T)\end{bmatrix}. \tag{14}$$

Now from (9), (13) and (14) it follows:

$$\mathbf{y}_k^*=\tilde{\mathbf{G}}\mathbf{x}(k\tau)+\tilde{\mathbf{H}}\mathbf{u}_\tau(k\tau)+\bar{\mathbf{H}}\mathbf{u}_k^*+\tilde{\mathbf{W}}\mathbf{d}(k\tau), \tag{15}$$

where

$$\mathbf{u}_k^*=\begin{bmatrix}\mathbf{u}_T(k\tau)\\ \mathbf{u}_T(k\tau+T)\\ \mathbf{u}_T(k\tau+2T)\\ \vdots\\ \mathbf{u}_T(k\tau+(N-3)T)\\ \mathbf{u}_T(k\tau+(N-2)T)\end{bmatrix},\ \tilde{\mathbf{G}}=\begin{bmatrix}\mathbf{C}\\ \mathbf{C}\mathbf{G}_T\\ \mathbf{C}\mathbf{G}_T^2\\ \vdots\\ \mathbf{C}\mathbf{G}_T^{N-2}\\ \mathbf{C}\mathbf{G}_T^{N-1}\end{bmatrix},$$

$$\tilde{\mathbf{H}}=\begin{bmatrix}\mathbf{0}\\ \mathbf{C}\mathbf{H}_T\\ \mathbf{C}(\mathbf{G}_T\mathbf{H}_T+\mathbf{H}_T)\\ \vdots\\ \mathbf{C}\sum_{i=0}^{N-3}\mathbf{G}_T^i\mathbf{H}_T\\ \mathbf{C}\sum_{i=0}^{N-2}\mathbf{G}_T^i\mathbf{H}_T\end{bmatrix},\ \tilde{\mathbf{W}}=\begin{bmatrix}\mathbf{0}\\ \mathbf{C}\mathbf{W}_T\\ \mathbf{C}(\mathbf{G}_T\mathbf{W}_T+\mathbf{W}_T)\\ \vdots\\ \mathbf{C}\sum_{i=0}^{N-3}\mathbf{G}_T^i\mathbf{W}_T\\ \mathbf{C}\sum_{i=0}^{N-2}\mathbf{G}_T^i\mathbf{W}_T\end{bmatrix}, \tag{16}$$

$$\bar{\mathbf{H}}=\begin{bmatrix}\mathbf{0} & \mathbf{0} & \cdots & \mathbf{0} & \mathbf{0}\\ \mathbf{C}\mathbf{H}_T & \mathbf{0} & \cdots & \mathbf{0} & \mathbf{0}\\ \mathbf{C}\mathbf{G}_T\mathbf{H}_T & \mathbf{C}\mathbf{H}_T & \cdots & \mathbf{0} & \mathbf{0}\\ \vdots & \vdots & \ddots & \vdots & \vdots\\ \mathbf{C}\mathbf{G}_T^{N-3}\mathbf{H}_T & \mathbf{C}\mathbf{G}_T^{N-4}\mathbf{H}_T & \cdots & \mathbf{C}\mathbf{H}_T & \mathbf{0}\\ \mathbf{C}\mathbf{G}_T^{N-2}\mathbf{H}_T & \mathbf{C}\mathbf{G}_T^{N-3}\mathbf{H}_T & \cdots & \mathbf{C}\mathbf{G}_T\mathbf{H}_T & \mathbf{C}\mathbf{H}_T\end{bmatrix}.$$

Matrices $\tilde{\mathbf{G}}$ and $\tilde{\mathbf{W}}$ may not be square, so Eq. (15) could have multiple solutions. In that case, Moore-Penrose matrix pseudoinverse is used in estimation algorithm instead of the regular inverse. Pseudoinverse of matrix $\mathbf{M}$ is defined as [38]:

$$\mathbf{M}^+=(\mathbf{M}^T\mathbf{M})^{-1}\mathbf{M}^T. \tag{17}$$

Eq. (15) can be directly used only for disturbance estimation:

$$\hat{\mathbf{d}}(k\tau)=\tilde{\mathbf{W}}^+\left(\mathbf{y}_k^*-\tilde{\mathbf{G}}\mathbf{x}(k\tau)-\tilde{\mathbf{H}}\mathbf{u}_\tau(k\tau)-\bar{\mathbf{H}}\mathbf{u}_k^*\right), \tag{18}$$

The usage of matrix's pseudoinverse will ensure that estimated values represent the least square solution of (15) [39].

Nevertheless, if Eq. (15) is also used for state estimation, estimated value would be delayed one sampling period τ. Therefore, for state estimation, that equation is combined with discrete systems dynamics (9), which results in the following state estimation:

$$\begin{aligned}\hat{\mathbf{x}}((k+1)\tau) &= \mathbf{G}_\tau\tilde{\mathbf{G}}^+\mathbf{y}_k^*+\mathbf{H}_\tau\mathbf{u}_\tau(k\tau)-\mathbf{G}_\tau\tilde{\mathbf{G}}^+\bar{\mathbf{H}}\mathbf{u}_k^*\\ &\quad +\mathbf{H}^\circ\mathbf{u}^\circ{}_k+(\mathbf{W}_\tau-\mathbf{G}_\tau\tilde{\mathbf{G}}^+\tilde{\mathbf{W}})\mathbf{d}(k\tau),\end{aligned} \tag{19}$$

where

$$\begin{aligned}\mathbf{H}^\circ &= [\mathbf{G}_T^{N-1}\mathbf{H}_T\quad \mathbf{G}_T^{N-2}\mathbf{H}_T\quad \cdots\quad \mathbf{G}_T\mathbf{H}_T\quad \mathbf{H}_T],\\ \mathbf{u}^\circ{}_k &= \begin{bmatrix}\mathbf{u}_T(k\tau)\\ \mathbf{u}_T(k\tau+T)\\ \mathbf{u}_T(k\tau+2T)\\ \vdots\\ \mathbf{u}_T(k\tau+(N-2)T)\\ \mathbf{u}_T(k\tau+(N-1)T)\end{bmatrix}.\end{aligned} \tag{20}$$

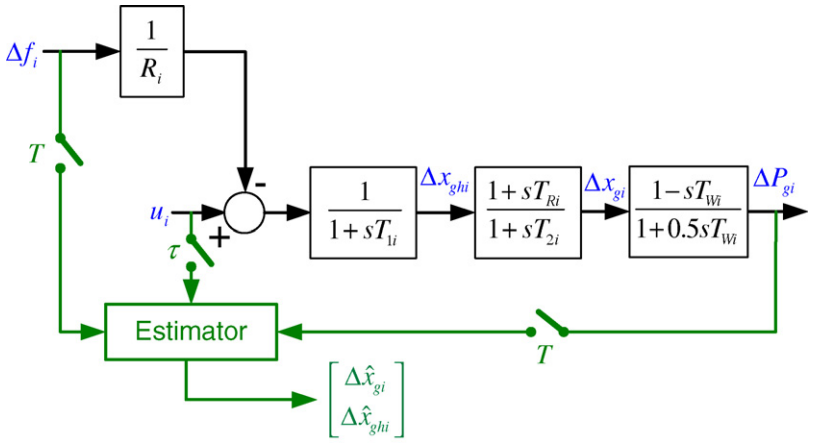

Fig. 5. A dynamical subsystem for state estimation.

3.2. Power system's state estimation

To estimate system state of a CA represented with substitute hydro power plant (Fig. 2), FOS is used. FOS is applied only to the subsystem of the power plant model, which is shown in Fig. 5, while the values of state, input and output vectors in (15) are shown in Table 2 (for this case unmeasured system state is Δx_{gi} and Δx_{ghi}, sampled input is $u_i(k\tau)$, subsampled input is $\Delta f_i(kT)$ and the output is $\Delta P_{gi}(kT)$). In this subsystem, there are no disturbances present. Because matrix $\tilde{\mathbf{G}}$ is generally not a regular square matrix, there may be many solutions of (15), so matrix pseudoinverse is used. The estimated state, computed by Eq. (19), is:

$$\begin{bmatrix} \Delta\hat{P}_{gi}(k\tau) \\ \Delta\hat{x}_{gi}(k\tau) \\ \Delta\hat{x}_{ghi}(k\tau) \end{bmatrix} = \mathbf{G}_{\tau i}\tilde{\mathbf{G}}_i^{+}\Delta\mathbf{P}^{*}_{g(k-1)i} + \mathbf{H}_{\tau i}\mathbf{u}_i((k-1)\tau) - \mathbf{G}_{\tau i}\tilde{\mathbf{G}}_i^{+}\tilde{\mathbf{H}}_i\Delta\mathbf{f}^{*}_{(k-1)i} + \mathbf{H}^{\circ}{}_i\Delta\mathbf{f}^{\circ}{}_{(k-1)i}, \quad (21)$$

where subscript $i = 2, 3$ (according to Fig. 1).

Similar procedure can be used to estimate unmeasurable system state of a CA represented with substitute thermal power plant (Fig. 3). The unmeasured system state is now Δx_{gi}, while all other substitute values are equal to those for system with substitute hydro power plant. Estimation equation for that case is:

$$\begin{bmatrix} \Delta\hat{P}_{gi}(k\tau) \\ \Delta\hat{x}_{gi}(k\tau) \end{bmatrix} = \mathbf{G}_{\tau i}\tilde{\mathbf{G}}_i^{+}\Delta\mathbf{P}^{*}_{g(k-1)i} + \mathbf{H}_{\tau i}\mathbf{u}_i((k-1)\tau) - \mathbf{G}_{\tau i}\tilde{\mathbf{G}}_i^{+}\tilde{\mathbf{H}}_i\Delta\mathbf{f}^{*}_{(k-1)i} + \mathbf{H}^{\circ}{}_i\Delta\mathbf{f}^{\circ}{}_{(k-1)i}, \quad (22)$$

where subscript $i = 1, 4$ (according to Fig. 1).

Values of estimated generator output power deviations, $\Delta\hat{P}_{gi}$, calculated by (21) or (22), are not used in the control algorithm, but their measured values are used there instead.

Table 2
Substitute matrices in (19) for state estimation.

Value in (19)	Substitute value
$\hat{\mathbf{x}}$	$\begin{bmatrix} \Delta\hat{P}_{gi} \\ \Delta\hat{x}_{gi} \\ \Delta\hat{x}_{ghi} \end{bmatrix}$ or $\begin{bmatrix} \Delta\hat{P}_{gi} \\ \Delta\hat{x}_{gi} \end{bmatrix}$
$\mathbf{y}^{*}$	$\Delta\mathbf{P}^{*}_{gi}$
$\mathbf{u}_{\tau}$	u_i
$\mathbf{u}^{*}, \mathbf{u}^{\circ}, \mathbf{u}_T$	$\Delta\mathbf{f}^{*}_i, \Delta\mathbf{f}^{\circ}{}_i, \Delta f_i$
$\mathbf{d}$	–

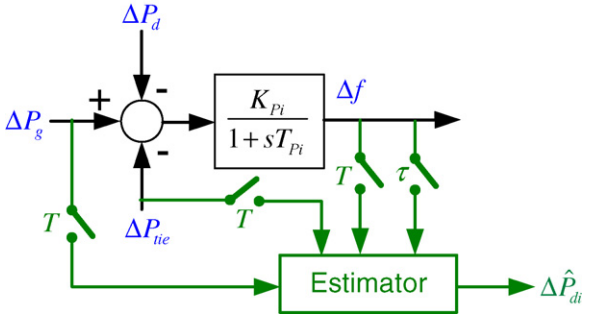

Fig. 6. A dynamical subsystem for disturbance estimation.

3.3. Power system's disturbance estimation

To estimate disturbance ΔP_d in CAs shown in Figs. 2 and 3, FOS is applied only to the subsystem shown in Fig. 6. In this case the substitute values of matrices in (15) are shown in Table 3 (system state is $\Delta f_i(k\tau)$, output is $\Delta f_i(kT)$, subsampled input is $\Delta P_{gi}(kT) - \Delta P_{tiei}(kT)$ and the disturbance is $\Delta P_{di}(kT)$). In this case, there is no input signal with sample period τ present in the subsystem.

The estimated disturbance, computed by Eq. (18),is:

$$\Delta\hat{P}_{di}(k\tau) = \tilde{\mathbf{W}}_i^{+}\left[\Delta\mathbf{f}^{*}_{ki} - \tilde{\mathbf{G}}_i\Delta f_i(k\tau) - \tilde{\mathbf{H}}_i(\Delta\mathbf{P}^{*}_{gki} - \Delta\mathbf{P}^{*}_{tieki})\right], \quad (23)$$

where subscript $i = 1, \ldots, 4$, since this disturbance estimation algorithm is independent of substitute power plant type.

Because it is assumed that disturbance has a constant value during the whole sampling period τ and because pseudoinverse matrix is used, the mean value of disturbance signal during the sampling period τ is calculated by Eq. (23).

With (21) or (22) and (23), both, full system state $\mathbf{x}(k\tau)$ and disturbance $\mathbf{d}(k\tau)$ are estimated. Therefore, a state based sliding mode LFC controller can be designed.

Table 3
Substitute matrices in (18) for disturbance estimation.

Value in (18)	Substitute value
$\mathbf{x}$	Δf_i
$\mathbf{y}^{*}$	$\Delta\mathbf{f}^{*}_i$
$\mathbf{u}_{\tau}$	–
$\mathbf{u}^{*}, \mathbf{u}_T$	$\Delta\mathbf{P}^{*}_{gi} - \Delta\mathbf{P}^{*}_{tiei}, \Delta P_{gi} - \Delta P_{tiei}$
$\mathbf{d}$	ΔP_{di}

4. Discrete-time sliding mode control and its application to LFC

Sliding mode control is a control technique appropriate for controlling time-variant systems in the presence of external disturbances. SMC based only on output signal cannot be used for systems with non-minimum phase behavior, because it leads to instability [35]. As seen from Fig. 2, a hydro power plant is a system with non-minimum phase behavior. Therefore, SMC based on full system state must be used in this case. To improve overall system behavior, disturbance is also included into controller's design. Because all state and disturbance are not measurable, estimation technique described in Section 3 is used to obtain their unmeasured components.

4.1. Sliding mode control for systems with uncertainties

Eq. (8) describes a linear time-invariant (LTI) system model in the presence of external disturbance. But in real systems there are many uncertainties present, which are caused by unmodelled dynamics or variations of system parameters. They can highly affect system's behavior.

A continuous LTI system (8) with additive uncertainties is described as:

$$\dot{\mathbf{x}}(t) = \mathbf{A}\mathbf{x}(t) + \mathbf{B}\mathbf{u}(t) + \mathbf{F}\mathbf{d}(t) + \boldsymbol{\xi}(\mathbf{x}, \mathbf{u}, t). \tag{24}$$

One way to categorize uncertainties in the system is into matched or unmatched uncertainties [40]. A condition that defines matched uncertainties is:

$$\boldsymbol{\xi}_m(\mathbf{x}, \mathbf{u}, t) \in \mathcal{R}(\mathbf{B}), \tag{25}$$

whereas all other uncertainties are unmatched. Because of the matching condition (25), matched uncertainties can be written as:

$$\boldsymbol{\xi}_m(\mathbf{x}, \mathbf{u}, t) = \mathbf{B}\boldsymbol{\gamma}, \tag{26}$$

where $\boldsymbol{\gamma} \in \mathbb{R}^m$ [40].

For better insight into system dynamics with SMC and for simpler controller synthesis it is more convenient to transform the system (24) into a regular canonical form [33]:

$$\begin{bmatrix} \dot{\mathbf{x}}_{c1}(t) \\ \dot{\mathbf{x}}_{c2}(t) \end{bmatrix} = \begin{bmatrix} \mathbf{A}_{11} & \mathbf{A}_{12} \\ \mathbf{A}_{21} & \mathbf{A}_{22} \end{bmatrix} \begin{bmatrix} \mathbf{x}_{c1}(t) \\ \mathbf{x}_{c2}(t) \end{bmatrix} + \begin{bmatrix} \mathbf{0} \\ \mathbf{B}_2 \end{bmatrix} \mathbf{u}(t) + \begin{bmatrix} \mathbf{F}_1 \\ \mathbf{F}_2 \end{bmatrix} \mathbf{d}(t) + \begin{bmatrix} \boldsymbol{\xi}_u(\mathbf{x}, t) \\ \boldsymbol{\xi}_m(\mathbf{x}, \mathbf{u}, t) \end{bmatrix}, \tag{27}$$

where $\mathbf{x}_{c1}$ and $\mathbf{x}_{c2}$ represent state vectors of the decoupled subsystems of system (24). In regular form system's uncertainties are decoupled into matched and unmatched ones.

As it can be seen from (27), the influence of matched uncertainties in continuous SMC can be fully compensated with proper control signal, which is not the case for unmatched uncertainties.

System's transformation into regular form can be done with nonsingular transformation matrix $\mathbf{T}_{cr}$, where matrices defining the transformed system can be obtained from the original system as:

$$\begin{aligned} \mathbf{x}_{cr}(t) &= \begin{bmatrix} \mathbf{x}_{c1}(t) \\ \mathbf{x}_{c2}(t) \end{bmatrix} = \mathbf{T}_{cr}\mathbf{x}(t), \\ \mathbf{A}_r &= \begin{bmatrix} \mathbf{A}_{11} & \mathbf{A}_{12} \\ \mathbf{A}_{21} & \mathbf{A}_{22} \end{bmatrix} = \mathbf{T}_{cr}\mathbf{A}\mathbf{T}_{cr}^{-1}, \\ \mathbf{B}_r &= \begin{bmatrix} \mathbf{0} \\ \mathbf{B}_2 \end{bmatrix} = \mathbf{T}_{cr}\mathbf{B}, \mathbf{F}_r = \begin{bmatrix} \mathbf{F}_1 \\ \mathbf{F}_2 \end{bmatrix} = \mathbf{T}_{cr}\mathbf{F}. \end{aligned} \tag{28}$$

SMC design procedure is shown in Fig. 7. It consists of two major steps: (1) selecting a sliding surface and (2) computing a control law that will force system's trajectory towards the chosen surface. A sliding surface will be selected for continuous time system in regular form, because then sliding surface's dependency upon system parameters in (3) or (6) is preserved. Because of the controller's discrete-time implementation, a control law will be computed for discrete-time system in regular form.

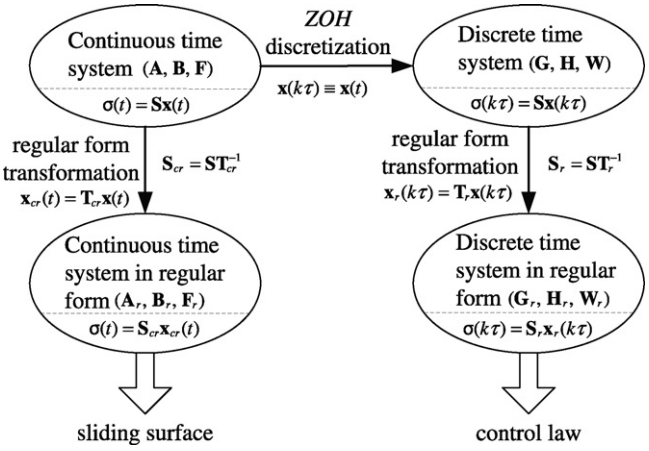

Fig. 7. SMC computation scheme.

4.2. A sliding surface

The first step in SMC controller synthesis is choosing a sliding surface, which defines desired system dynamics:

$$\boldsymbol{\sigma}(\mathbf{x}) = \mathbf{S}\mathbf{x} = \mathbf{0}, \tag{29}$$

where $\mathbf{S} \in \mathbb{R}^{m \times n}$ is a switching matrix.

The aim of SMC is to force the state, firstly to reach, and then to stay on the sliding surface. According to that, system trajectory in SMC consists of two phases: a reaching phase and a sliding phase. SMC is forcing system's trajectory towards the surface by switching between different controller structures, depending on the sign of a switching function. The switching function is defined as:

$$\boldsymbol{\sigma}(t) = \mathbf{S}\mathbf{x}(t). \tag{30}$$

It is important to distinguish the sliding surface $\boldsymbol{\sigma}(\mathbf{x}) = \mathbf{0}$, which is time-independent manifold in state space and the switching function $\boldsymbol{\sigma}(t)$, which is time-dependent function of system state's position regarding to the sliding surface.

For the system in regular form (27), switching function becomes:

$$\boldsymbol{\sigma}(t) = \mathbf{S}_{c1}\mathbf{x}_{c1}(t) + \mathbf{S}_{c2}\mathbf{x}_{c2}(t), \tag{31}$$

where

$$\mathbf{S}_{cr} = \begin{bmatrix} \mathbf{S}_{c1} & \mathbf{S}_{c2} \end{bmatrix} = \mathbf{S}\mathbf{T}_{cr}^{-1}. \tag{32}$$

System dynamics in the sliding mode are obtained from (27) and (31):

$$\begin{bmatrix} \dot{\mathbf{x}}_{c1}(t) \\ \dot{\boldsymbol{\sigma}}(t) \end{bmatrix} = \begin{bmatrix} \hat{\mathbf{A}}_{11} & \hat{\mathbf{A}}_{12} \\ \hat{\mathbf{A}}_{21} & \hat{\mathbf{A}}_{22} \end{bmatrix} \begin{bmatrix} \mathbf{x}_1(t) \\ \boldsymbol{\sigma}(t) \end{bmatrix} + \begin{bmatrix} \mathbf{0} \\ \hat{\mathbf{B}}_2 \end{bmatrix} \mathbf{u}(t) + \begin{bmatrix} \mathbf{F}_1 \\ \hat{\mathbf{F}}_2 \end{bmatrix} \mathbf{d}(t) + \begin{bmatrix} \boldsymbol{\xi}_u(\mathbf{x}, t) \\ \boldsymbol{\xi}_s(\mathbf{x}, \mathbf{u}, t) \end{bmatrix}. \tag{33}$$

where

$$\begin{aligned}
\hat{\mathbf{A}}_{11} &= \mathbf{A}_{11} - \mathbf{A}_{12}\mathbf{S}_c^*,\\
\hat{\mathbf{A}}_{12} &= \mathbf{A}_{12}\mathbf{S}_{c2}^{-1},\\
\hat{\mathbf{A}}_{21} &= \mathbf{S}_{c1}\mathbf{A}_{11} - \mathbf{S}_{c1}\mathbf{A}_{12}\mathbf{S}_c^* + \mathbf{S}_{c2}\mathbf{A}_{21} - \mathbf{S}_{c2}\mathbf{A}_{22}\mathbf{S}_c^*,\\
\hat{\mathbf{A}}_{22} &= \mathbf{S}_{c1}\mathbf{A}_{12}\mathbf{S}_{c2}^{-1} + \mathbf{S}_{c2}\mathbf{A}_{22}\mathbf{S}_{c2}^{-1},\\
\hat{\mathbf{B}}_2 &= \mathbf{S}_{c2}\mathbf{B}_2,\\
\hat{\mathbf{F}}_2 &= \mathbf{S}_{c1}\mathbf{F}_1 + \mathbf{S}_{c2}\mathbf{F}_2,\\
\boldsymbol{\xi}_s(\mathbf{x},\mathbf{u},t) &= \mathbf{S}_{c1}\boldsymbol{\xi}_u(\mathbf{x},t) + \mathbf{S}_{c2}\boldsymbol{\xi}_m(\mathbf{x},\mathbf{u},t),\\
\mathbf{S}_c^* &= \mathbf{S}_{c2}^{-1}\mathbf{S}_{c1}.
\end{aligned} \tag{34}$$

The term $\boldsymbol{\xi}_s(\mathbf{x},\mathbf{u},t)$ in (33) and (34) denotes sliding uncertainties, which can be defined as the total influence of uncertainties to the dynamics of reaching the sliding mode.

Including the condition for sliding mode ($\boldsymbol{\sigma}(t)=\mathbf{0}$) into the system (33), the dynamics of the system in sliding mode become:

$$\dot{\mathbf{x}}_{c1}(t) = \hat{\mathbf{A}}_{11}\mathbf{x}_1(t) + \mathbf{F}_1\mathbf{d}(t) + \boldsymbol{\xi}_u(\mathbf{x},t). \tag{35}$$

From (35) two improvements in system behavior can be noted. One is that the order of system dynamics is reduced compared to the original system (27). The reduction factor is m, which is a dimension of the control signal $\mathbf{u}(t)$. The other improvement is system's invariance to matched uncertainties, as they are not present in (35).

Remark 1. *For discrete-time systems those improvements are not fully valid. Due to discrete control signal, system trajectory can not be held strictly on the surface and matched uncertainties can influence the systems dynamics. Nevertheless, if the boundedness of uncertainties is conserved, system trajectory will maintain inside a narrow band in the vicinity of the sliding surface.*

Switching matrix $\mathbf{S}$ in (29) must be chosen such that the system in sliding mode is stable, i.e. all eigenvalues of matrix $\hat{\mathbf{A}}_{11}$ must be in the left complex halfplane.

In LFC it is required for system output i.e. ACE signal in steady state to be equal to zero. In sliding mode system output in steady state depends upon parameters of the switching matrix $\mathbf{S}$ [41]. Therefore, besides ensuring system's stability in sliding mode, matrix $\mathbf{S}$ should be chosen such to minimize system's steady state error.

4.3. A control law

A control law will be computed for discrete-time ZOH approximation of continuous-time LTI system with uncertainties (24):

$$\mathbf{x}((k+1)\tau) = \mathbf{G}\mathbf{x}(k\tau) + \mathbf{H}\mathbf{u}(k\tau) + \mathbf{W}\mathbf{d}(k\tau) + \boldsymbol{\xi}(\mathbf{x},\mathbf{u},k\tau), \tag{36}$$

where matrices $\mathbf{G}$, $\mathbf{H}$ and $\mathbf{W}$ are obtained from (10). For control law computation discrete-time systems (36) is firstly transformed into regular form using nonsingular transformation matrix $\mathbf{T}_r$. Transformation procedure is similar to the one described for continuous-time system.

For the system in regular form, the switching function is defined as:

$$\boldsymbol{\sigma}(k\tau) = \mathbf{S}_1\mathbf{x}_1(k\tau) + \mathbf{S}_2\mathbf{x}_2(k\tau), \tag{37}$$

where

$$\mathbf{S}_r = \begin{bmatrix}\mathbf{S}_1 & \mathbf{S}_2\end{bmatrix} = \mathbf{S}\mathbf{T}_r^{-1}. \tag{38}$$

Combining discrete-time system in regular form and Eq. (37), system dynamics in the sliding mode are obtained as:

$$\begin{aligned}
\begin{bmatrix}\mathbf{x}_1((k+1)\tau)\\ \boldsymbol{\sigma}((k+1)\tau)\end{bmatrix} = &\begin{bmatrix}\hat{\mathbf{G}}_{11} & \hat{\mathbf{G}}_{12}\\ \hat{\mathbf{G}}_{21} & \hat{\mathbf{G}}_{22}\end{bmatrix}\begin{bmatrix}\mathbf{x}_1(k\tau)\\ \boldsymbol{\sigma}(k\tau)\end{bmatrix} + \begin{bmatrix}\mathbf{0}\\ \hat{\mathbf{H}}_2\end{bmatrix}\mathbf{u}(k\tau)\\
&+ \begin{bmatrix}\mathbf{W}_1\\ \hat{\mathbf{W}}_2\end{bmatrix}\mathbf{d}(k\tau) + \begin{bmatrix}\boldsymbol{\xi}_u(\mathbf{x},k\tau)\\ \boldsymbol{\xi}_s(\mathbf{x},\mathbf{u},k\tau)\end{bmatrix}.
\end{aligned} \tag{39}$$

where

$$\begin{aligned}
\hat{\mathbf{G}}_{11} &= \mathbf{G}_{11} - \mathbf{G}_{12}\mathbf{S}^*,\\
\hat{\mathbf{G}}_{12} &= \mathbf{G}_{12}\mathbf{S}_2^{-1},\\
\hat{\mathbf{G}}_{21} &= \mathbf{S}_1\mathbf{G}_{11} - \mathbf{S}_1\mathbf{G}_{12}\mathbf{S}^* + \mathbf{S}_2\mathbf{G}_{21} - \mathbf{S}_2\mathbf{G}_{22}\mathbf{S}^*,\\
\hat{\mathbf{G}}_{22} &= \mathbf{S}_1\mathbf{G}_{12}\mathbf{S}_2^{-1} + \mathbf{S}_2\mathbf{G}_{22}\mathbf{S}_2^{-1},\\
\hat{\mathbf{H}}_2 &= \mathbf{S}_2\mathbf{H}_2,\\
\hat{\mathbf{W}}_2 &= \mathbf{S}_1\mathbf{W}_1 + \mathbf{S}_2\mathbf{W}_2,\\
\boldsymbol{\xi}_s(\mathbf{x},\mathbf{u},k\tau) &= \mathbf{S}_1\boldsymbol{\xi}_u(\mathbf{x},k\tau) + \mathbf{S}_2\boldsymbol{\xi}_m(\mathbf{x},\mathbf{u},k\tau)\\
\mathbf{S}^* &= \mathbf{S}_2^{-1}\mathbf{S}_1.
\end{aligned} \tag{40}$$

The control law will be computed according to (39), by an appropriate choice of a reaching law. The reaching law is in charge of driving system trajectory to the sliding surface $\boldsymbol{\sigma}(\mathbf{x})=\mathbf{0}$. Among several known reaching laws [42–46], a linear reaching law from [46] is chosen to be used for LFC. It is defined as:

$$\boldsymbol{\sigma}(k+1) = \boldsymbol{\Lambda}\boldsymbol{\sigma}(k), \tag{41}$$

where $\boldsymbol{\Lambda}$ is a diagonal matrix whose elements are constrained to $0 \le \lambda_i < 1$.

When applied to the system (39) and with neglected uncertainties, reaching law (41) results with the following control law:

$$\mathbf{u}(k\tau) = \hat{\mathbf{H}}_2^{-1}\left[(\boldsymbol{\Lambda} - \hat{\mathbf{G}}_{22})\boldsymbol{\sigma}(k\tau) - \hat{\mathbf{G}}_{21}\mathbf{x}_1(k\tau) - \hat{\mathbf{W}}_2\mathbf{d}(k\tau)\right]. \tag{42}$$

Because uncertainties are neglected in the computation of the control law (42), the ideal sliding mode is not guaranteed. Instead of that, system trajectory will reside in a quasi sliding mode band, whose width, w_b, depends upon the value of components of sliding uncertainties vector, $\boldsymbol{\xi}_s(\mathbf{x},\mathbf{u},k\tau)$, and also upon the parameters of matrix $\boldsymbol{\Lambda}$ [35]:

$$w_b = \sqrt{\sum_{i=1}^{m}\left(\frac{1}{1-\lambda_i}\max(\xi_{si}(\mathbf{x},k\tau))\right)}. \tag{43}$$

As stated above, in LFC state and disturbance are not fully measurable, therefore their unmeasured values in (42) are substituted with the estimated values. Estimated states are obtained by (21) or (22), while estimated disturbances are obtained by (23). Estimated values are not exactly equal to the true values. The differences are caused by discretization (9) and by least square approximation which is obtained when matrix's pseudoinverse (17) is used. They are further included into the computation of control signal (42). Because those errors can also be seen as uncertainties in (24), their influence can be reduced by introducing sliding uncertainties estimation term into (42). Thus, the control law becomes:

$$\mathbf{u}(k\tau) = \hat{\mathbf{H}}_2^{-1}\left[(\boldsymbol{\Lambda} - \hat{\mathbf{G}}_{22})\boldsymbol{\sigma}(k\tau) - \hat{\mathbf{G}}_{21}\mathbf{x}_1(k\tau) - \hat{\mathbf{W}}_2\mathbf{d}(k\tau) - \hat{\boldsymbol{\xi}}_s(k\tau)\right], \tag{44}$$

where

$$\hat{\boldsymbol{\xi}}_s(k\tau) = \hat{\boldsymbol{\xi}}_s((k-1)\tau) + \boldsymbol{\sigma}(k\tau) - \boldsymbol{\Lambda}\boldsymbol{\sigma}((k-1)\tau). \tag{45}$$

When sliding uncertainties estimation is included into the control law computation, the width of the quasi sliding mode band becomes [35]:

$$w_b = \sqrt{\sum_{i=1}^{m} \left(\frac{1}{1-\lambda_i} \max(\Delta\xi_{si}(\mathbf{x}, k\tau)) \right)}, \tag{46}$$

where $\Delta\xi_{si}(\mathbf{x}, k\tau) = |\xi_{si}(\mathbf{x}, (k+1)\tau) - \xi_{si}(\mathbf{x}, k\tau)|$. The width of quasi sliding mode band in (43) is based on the maximal value of sliding uncertainties, while the width in (46) is based on the maximal rate of change of sliding uncertainties. Generally, the width (46) is much smaller.

Since the main task of the sliding mode controller is to steer the system towards the sliding surface, estimating sliding uncertainties instead of all system uncertainties is enough to obtain that task.

4.4. SMC application to LFC

Remark 2. *Because control signal in LFC has dimension one* ($m = 1$, $\mathbf{u} \equiv u$), *there is only one sliding surface. Therefore, switching matrix becomes a switching vector while reaching law matrix becomes a scalar* ($\mathbf{\Lambda} \equiv \lambda$).

According to (2), a switching vector for a CA with hydro power plant is:

$$\mathbf{S} = \begin{bmatrix} s_f & s_{Ptie} & s_{Pg} & s_{xg} & s_{xgh} \end{bmatrix}, \tag{47}$$

while according to (5), a switching vector for a CA with thermal power plant it is:

$$\mathbf{S} = \begin{bmatrix} s_f & s_{Ptie} & s_{Pg} & s_{xg} \end{bmatrix}. \tag{48}$$

The choice of parameters of switching vectors (47) and (48) must ensure system's stability in the sliding mode and it must also minimize ACE deviation in the steady state, which is the main goal of LFC.

Minimization of ACE in steady state sliding mode can be done either analytically [41,47] or with the usage of iterative heuristic algorithms [7,48]. In this paper, steady state ACE will be minimized analytically. Minimization procedure results in constraints that will be later incorporated into a genetic algorithm in charge of finding controller's optimal parameters (see Section 5).

The constraints will be computed separately for a CA with hydro power plant and for a CA with thermal power plant. To compute the constraints, the systems must be in regular form. A CA with thermal power plant, described with (6), is already in regular form, therefore $\mathbf{T}_{cr} = \mathbf{I}$. For a CA with hydro power plant transformation matrix is:

$$\mathbf{T}_{cr} = \begin{bmatrix} K_B & 1 & 0 & 0 & 0 \\ 0 & 1 & 0 & 0 & 0 \\ 0 & 0 & 1 & 2 & 0 \\ 0 & 0 & 0 & 1 & -\dfrac{T_R}{T_2} \\ 0 & 0 & 0 & 0 & 1 \end{bmatrix}. \tag{49}$$

Steady state ACE for system in regular form can be computed using (35) and neglecting uncertainties. In sliding mode's steady state it is $\dot{\mathbf{x}}_{c1}(t) = \mathbf{0}$, therefore ACE becomes:

$$ACE_{ss} = -\mathbf{C}_1 \hat{\mathbf{A}}_{11}^{-1} \mathbf{F}_1 \mathbf{d}(t), \tag{50}$$

where

$$\mathbf{C}_r = \begin{bmatrix} \mathbf{C}_1 & \mathbf{C}_2 \end{bmatrix} = \mathbf{C}\mathbf{T}_{cr}^{-1}. \tag{51}$$

For ACE_{ss} to be equal to zero for system in sliding mode regardless the value of disturbance, parameters of the switching vector must be chosen such that they ensure:

$$\mathbf{C}_1 \hat{\mathbf{A}}_{11}^{-1} \mathbf{F}_1 = \mathbf{0}. \tag{52}$$

Solving (52) for a CA with hydro power plant, the switching vector (47), and the transformation matrix (49) gives:

$$\begin{aligned} s_{Pg} + s_{xg} + s_{xgh} &= 0, \\ s_{Ptie} &\neq 0. \end{aligned} \tag{53}$$

Similarly, solving (52) for a CA with thermal power plant and the switching vector (48), while having in mind $\mathbf{T}_{cr} = \mathbf{I}$, gives:

$$\begin{aligned} s_{Pg} + s_{xg} &= 0, \\ s_{Ptie} &\neq 0. \end{aligned} \tag{54}$$

Inequality $s_{Ptie} \neq 0$ in (53) and (54) is a constraint introduced to avoid undefined solution of (52), $ACE_{ss} = 0/0$.

Altogether, parameters of the switching vector $\mathbf{S}$ must be chosen such that matrix $\hat{\mathbf{A}}_{11}$ is a Hurwitz matrix, while condition (53) or (54) must also be fulfilled.

5. GA for finding LFC controller's parameters

As it can be seen from (38), (40) and (44), apart from system parameters, control law depends on switching vector $\mathbf{S}$ and reaching law parameter λ. To determine their optimal values GA is used.

GA is a random search approach which imitates natural process of evolution. It is appropriate for finding global optimal solution inside a multidimensional searching space. GAs have been used to find parameters for different LFC algorithms, e.g. integral control [21] or variable structure control [7,32]. The main problem in applying SMC based LFC presented in [7,32] is that a rapidly changing continuous time control signal is used there. Unfortunately, that is impracticable in real power system and discrete-time control signal must be used instead.

Since scaling of the switching vector has no effect on the dynamics of the sliding motion [33], it can be assumed that switching vector parameter s_{Pg} in (47) and (48) is $s_{Pg} = 1$.

For a CA with hydro power plant GA should find optimal values of s_f, s_{Ptie}, s_{xg} and λ, while s_{xgh} can be computed from (53). Therefore, every chromosome in the population consists of four genes: s_f, s_{Ptie}, s_{xg} and λ.

For a CA with thermal power plant GA should find optimal values of s_f, s_{Ptie}, and λ, while from (54) it can be computed that $s_{xg} = -1$. Therefore, in this case every chromosome in the population consists of three genes: s_f, s_{Ptie} and λ.

A detailed flow chart of the GA used in this paper is shown in Fig. 8. From random initial population, GA starts a loop of evolution processes, consisting of selection, crossover and mutation, in order to improve the average fitness function of the whole population.

GA consists of the following steps:

(i) A random initial population is created.
(ii) For all chromosomes in the population a switching vector $\mathbf{S}$ in the form (47) or (48) is calculated and then it is transformed into regular form using (38).
(iii) Using (40), parameters of the control law (42) are calculated.
(iv) For every chromosome in the population that ensures all eigenvalues of the matrix $\hat{\mathbf{G}}_{11}$ from (39) are within the complex unit circle, fitness function is evaluated by simulation on the proposed power system model. The chromosome with the best fitness function is memorized and used again in step (viii) (elitism).
(v) Using roulette wheel selection [49], individual chromosomes are selected for creating the next generation.

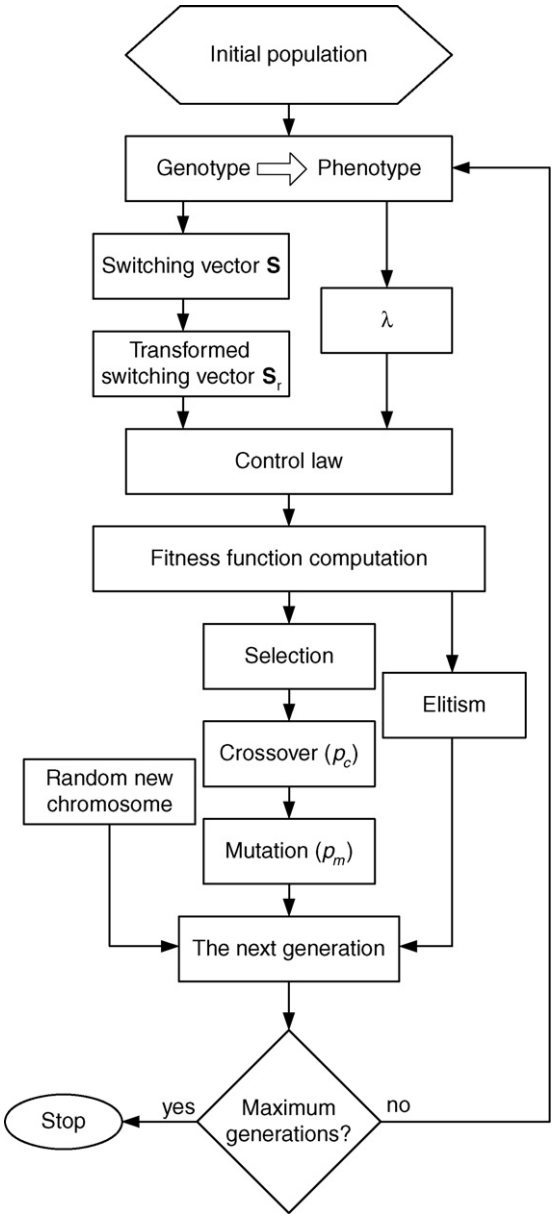

Fig. 8. Flow chart of GA algorithm.

(vi) Offsprings are created by the process of one-point crossover between selected chromosomes. The probability of crossover is p_c.
(vii) Some random bits of offspring chromosomes are mutated. The probability of mutation is p_m.
(viii) The next generation is composed of the obtained offsprings and of the best chromosome in the current generation (calculated in step (iv)).
(ix) Steps (ii)–(ix) are repeated until predefined number of generation has been produced.

Fitness function used in step (iv) is modified integral square of ACE and control signals:

$$J = \int_0^\infty (ACE(t))^2 dt + \mu(u(t))^2 dt, \tag{55}$$

where μ is a weighting factor.

Parameters used in GA are shown in Table 4.

Table 4
Parameters of the used genetic algorithm.

Parameter	Description	Value
N_{ch}	Chromosomes in the population	100
n_g	Genes in every chromosome	5
n_b	Bits in every gene	10
p_c	Probability of crossover	0.7
p_m	Probability of mutation	0.05
N_{GM}	Maximal number of generations	50

Instead of searching for the optimal values of sliding mode algorithm parameters throughout the vast space of possible solutions, this procedure reduces GA's searching space to significantly smaller subspace. Within that subspace, system stability and no steady state error is guarantied. This increases the possibility of finding global optimal solution instead of a local one.

If GA search algorithm for SMC based LFC parameters is compared to the search algorithm presented in [47], GA is able to find the optimal solution with smaller value of the fitness function, while having longer computation time. The reason is in GA's ability to escape from local extremes. Since the optimal controller parameters are computed off-line and only once, disadvantage regarding computation time can be neglected.

6. Simulation results

6.1. Simulation parameters

To test the proposed sliding mode algorithm, simulations of interconnected power system consisting of four CAs as shown in Fig. 1 were conducted. Parameters of the simulated system are given in Table 5 (most of them are from [21] and [29]). Sampling period of the control signal was $\tau = 1$ s and subsampling period of the output signals was $T = 0.2$ s, which satisfied observability indices constraints, therefore making matrix forms $(\mathbf{X}^T\mathbf{X})$ in (21)–(23) invertible.

We conducted simulations as follows. Firstly, to obtain fair comparison of the proposed SMC controller with the PI controller, parameters of PI controllers were obtained using GAs for all four CAs. Discrete-time PI controllers were used, where the control signal was obtained from system's output measurements as:

$$u(k\tau) = -\left(K_{pr}ACE(k\tau) + K_{int}\sum_{l=0}^{k} ACE(l\tau)\right). \tag{56}$$

Parameters of PI controllers were also chosen to minimize fitness function (55). The controller's parameters (proportional gain K_{pr} and integral gain K_{int}) are shown in Table 6.

Table 5
Parameters of interconnected power system model.

Parameter	Unit	Control area			
		CA1	CA2	CA3	CA4
K_P	[Hz/p.u.MW]	120	115	80	75
T_P	[s]	20	20	13	15
R	[Hz/p.u.MW]	2.4	2.5	3.3	3
K_B	[p.u.MW/Hz]	0.425	0.409	0.316	0.347
T_R	[s]	–	0.6	0.513	–
T_1	[s]	–	48.7	32	–
T_2	[s]	–	5	10	–
T_W	[s]	–	1	2	–
T_G	[s]	0.08	–	–	0.2
T_T	[s]	0.3	–	–	0.3
K_{S12}	[p.u.MW]	0.545			
K_{S14}	[p.u.MW]	0.5			
K_{S23}	[p.u.MW]	0.444			
K_{S34}	[p.u.MW]	0.545			

Table 6
Parameters of the optimal PI controllers.

Control area	K_{pr}	K_{int}
CA1	0.2605	0.4962
CA2	5.2951	0.0828
CA3	2.8426	0.0613
CA4	0.3218	0.7043

Table 7
Parameters of the the optimal SMC controllers.

Control area	S	λ
CA1	[−0.8858 −1.8804 1 −1]	0.9985
CA3	[−1.3797 10.0342 1 −16.7999 15.7999]	0.9969

Secondly, optimal SMC controller parameters for CA1 were obtained with optimal PI controllers used in other three CAs. Analogously, optimal SMC controller parameters in CA3 were obtained with optimal PI controllers used in CA1, CA2 and CA4. Controller parameters obtained with GAs for CA1 and CA3 are shown in Table 7. Weighting parameter μ in the fitness function (55) was set to $\mu = 0.01$.

Thirdly, the interconnection scheme was simulated with simultaneous use of the SMC controllers in CA1 and CA3.

During the simulation, four step disturbances were generated, one in each CA: $\Delta P_{d1} = 1\%$ p.u.MW, at $t = 1$ s, $\Delta P_{d2} = -1\%$ p.u.MW, at $t = 120$ s, $\Delta P_{d3} = 1\%$ p.u.MW, at $t = 360$ s and $\Delta P_{d4} = -1\%$ p.u.MW, at $t = 600$ s. The disturbances in neighbor CAs were generated to test the overall power system behavior.

6.2. Estimations

Estimation of disturbances and unmeasured states were obtained using (21)–(23). For CA1, true and estimated disturbance signals during the first three minutes are shown in Fig. 9. For CA3 true and estimated governor valve position deviation ($\Delta x_g(t)$) and governor valve servomotor position deviation ($\Delta x_{gh}(t)$) signals throughout the seventh minute are shown in Fig. 10.

It can be seen from the figures that state estimation is very good in the sampling instants. Disturbance estimation is slightly poorer, especially right after the disturbances occur, but estimation errors disappear with time. The reason for that is the fact that system dynamics within period τ are included in state estimation, while the disturbance is presumed constant during that period.

6.3. Load-frequency control

ACE signals with the optimal SMC controller parameters in CA1 and CA3 and with the optimal PI controller parameters in CA2 and CA4 are shown in Fig. 11. Control laws are given with (44) and (56). It can be observed from the figure that controllers in all four CAs regulate ACE signals to zero after the disturbances occur (it can also be noted that in all four CAs it is in steady state $ACE_{ss} = 0$).

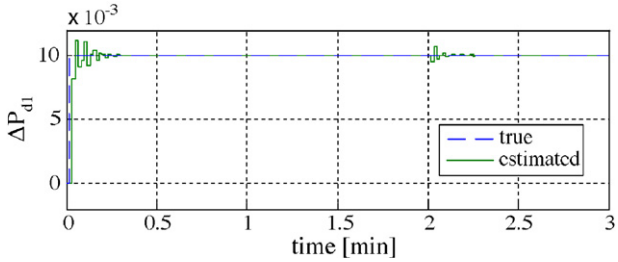

Fig. 9. True and estimated disturbance in CA1.

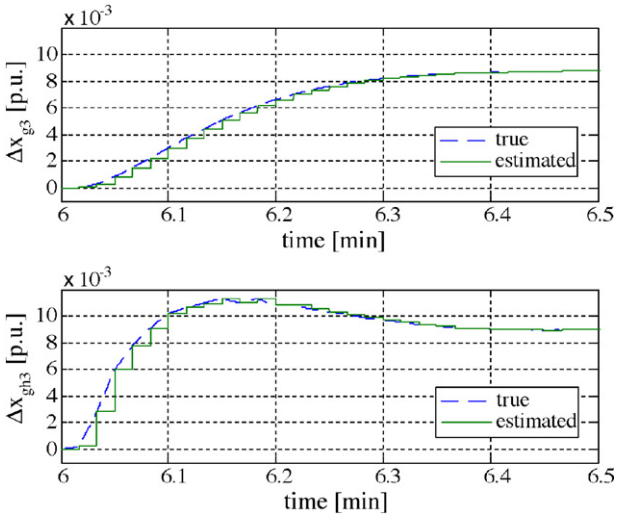

Fig. 10. True and estimated state in CA3.

Due to smaller time constants in thermal power plants, disturbance compensation in CA1 and CA4 is much faster than in CA2 and CA3.

Switching functions (29) in CA1 and CA3 are shown in Fig. 12. It can be seen from the figure that the system tends to return into sliding mode after the disturbances occur.

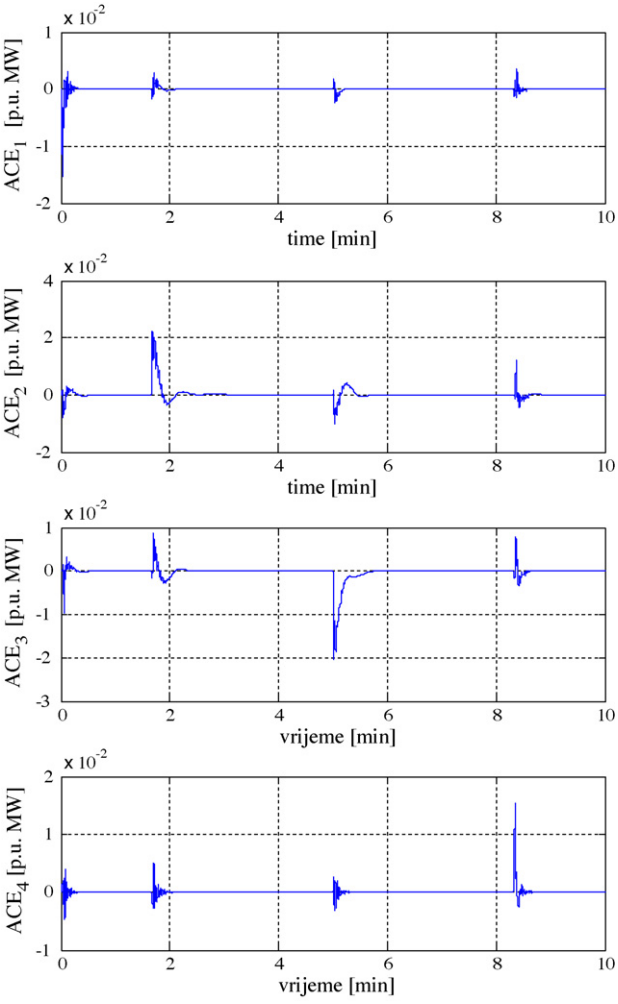

Fig. 11. ACE signals in interconnected power system.

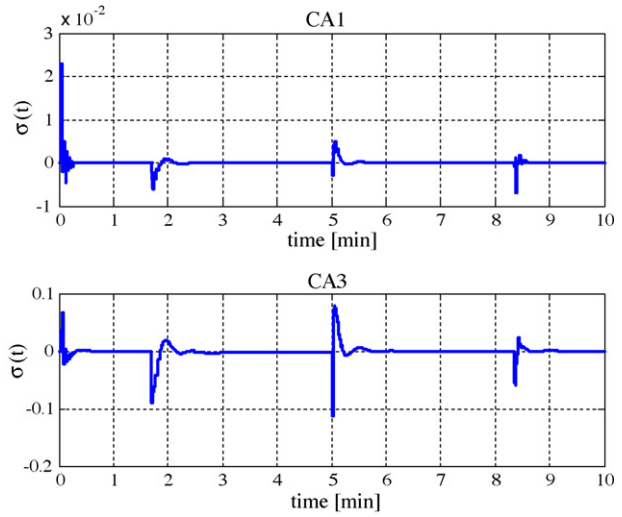

Fig. 12. Switching function in areas with sliding mode controllers.

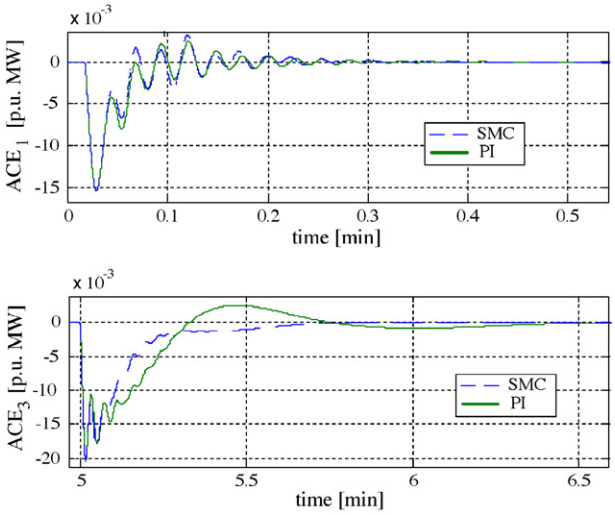

Fig. 13. ACE with SMC and PI controller.

A comparison of sliding mode based controller and PI controller is shown in Fig. 13. It can be seen from the figure that SMC and PI controllers give similar behavior in CA1 (thermal power plant), while in CA3 (hydro power plant) SMC gives better behavior than PI controller, i.e. it gives system response without overshoot and with shorter settling time. Therefore, this control algorithm is appropriate for controlling CAs which have mostly hydro power plants engaged in load-frequency control.

6.4. SMC and PI based LFC with nonlinearities in the model

Although linearized models are used for controllers synthesis, in real power plants there are many nonlinearities present. It is the most common to consider the effects of generation rate constraint (GRC) and of governor deadband (GDB) [16,23,50,51]. A thermal power plant model with included GRC and GDB is shown in Fig. 14, while hydro power plant with same nonlinearities is shown in Fig. 15.

In simulations, GRC was set to ±0.0017 p.u.MW/s for thermal power plants and ±0.045 p.u.MW/s for hydro power plants. Backlash width of GDB was set to $D = 0.04\%$ for both, thermal and hydro power plants [7].

To compare SMC and PI based LFC for model with nonlinearities, system behavior was tested against a larger disturbance $\Delta P_{di} = 10\%$ p.u.MW in CA1 and CA3. In Fig. 16 ACE in CA1 and CA3 for system with nonlinearities and both controllers is shown.

Switching functions (29) in CA1 and CA3 for system with nonlinearities are shown in Fig. 17.

Because PI controller is designed for the vicinity around an operating point, its behavior is significantly degraded when system differs from that operating point. That deviation from the operating point is caused by large disturbance. In CA1 PI controller causes significant oscillations due to nonlinearities [50], while with SMC controller those oscillation are damped. Nevertheless, SMC based controller shows good behavior even when system is not in the vicinity of the operation point. The reason for that is its robustness to uncertainties. Nonlinear system model shows that SMC based controller is superior to PI controller for both, thermal and hydro substitute power plant.

The only drawback of SMC based controller is that it can not force ACE signal to be equal to zero in steady state, instead the controller keeps it in narrow zone around zero. Width of that zone is determined by uncertainties in the system. As it is seen in Fig. 17, adding only estimation of sliding uncertainties into control law computation results in very narrow quasi sliding mode band. Since

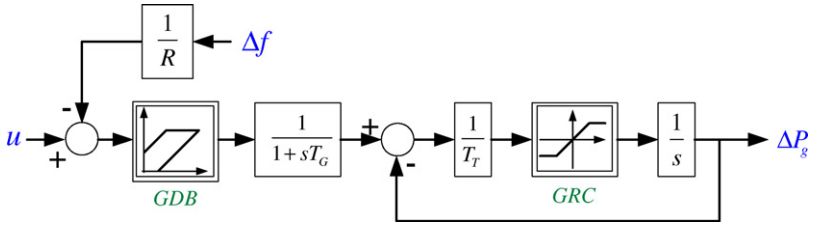

Fig. 14. Thermal power plant with nonlinearities.

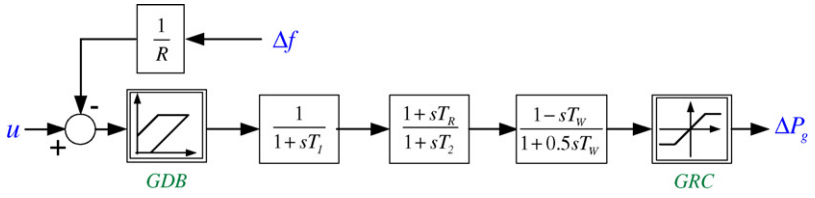

Fig. 15. Hydro power plant with nonlinearities.

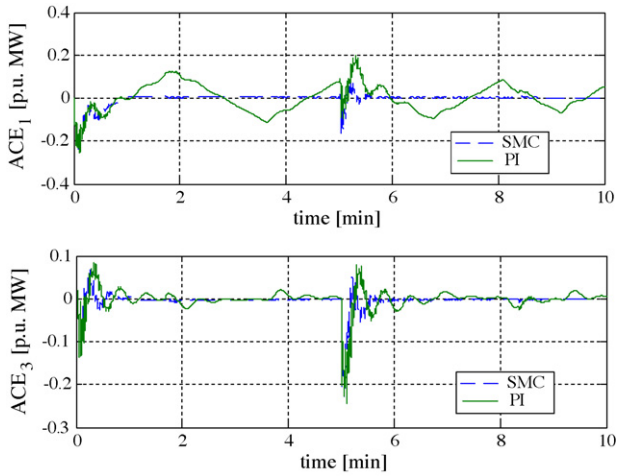

Fig. 16. ACE in CA1 and CA3 for system with included nonlinearities.

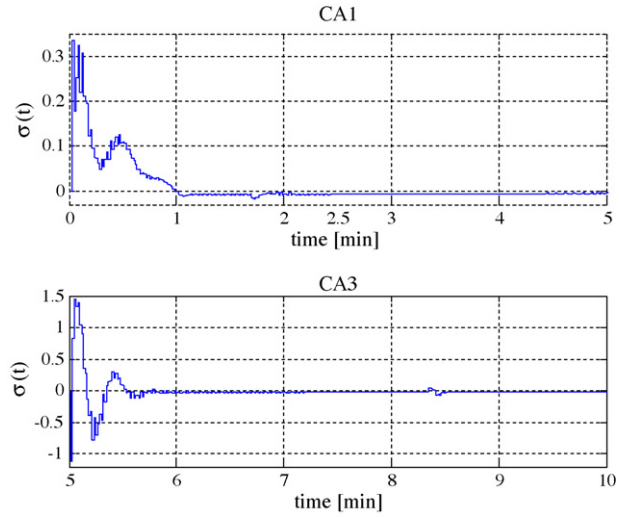

Fig. 17. Switching function in areas with sliding mode controllers in the presence of nonlinearities.

UCTE defines allowable absolute frequency deviation from its nominal up to 50 mHz during normal system operation [1], there is no need to include estimation of unmatched uncertainties into control algorithm. If that would be needed for the implementation of this algorithm in real power system, a good method can be found in [52].

7. Conclusion

In this paper, a design method of discrete-time sliding mode based load-frequency controller for power system is presented. Controller is designed for both power system represented with hydro and with thermal power plant. Since sliding mode controller needs full-state feedback, all unmeasured system states and disturbance are estimated by the method based on fast sampling of measured system variables. Parameters of the controllers are tuned using GAs in a way to minimize integral square of the area control error and control signal. The proposed controller is validated through simulations on linear and nonlinear power system models consisting of four different control areas. Simulation results obtained on linear power system model show that the proposed sliding mode based load frequency control outperforms conventional PI based load-frequency control regarding dynamical behavior for control areas represented with hydro power plat. Simulation results obtained on nonlinear power system model show that sliding mode based load-frequency control significantly outperforms conventional PI based load frequency control regarding damping of the oscillation caused by nonlinearities, for both types of power plants.

Acknowledgement

This research was supported by Končar - Power Plant and Electric Traction Engineering Inc., Zagreb, Croatia, and Ministry of Science, Education and Sports of the Republic of Croatia.

References

[1] UCTE, Operational handbook—load-frequency control and performance, 2004, http://www.ucte.org.
[2] A. Germond, R. Podmore, Dynamic aggregation of generating unit models, IEEE Transactions on Power Apparatus and Systems-97 (4) (1978) 1060–1069.
[3] B. Stojkovic, An original approach for load-frequency control—the winning solution in the second UCTE synchronous zone, Electric Power Systems Research 69 (1) (2004) 59–68.
[4] D. Iracleous, A. Alexandridis, A multi-task automatic generation control for power regulation, Electric Power Systems Research 73 (3) (2005) 275–285.
[5] H. Bevrani, T. Hiyama, Robust decentralised PI based LFC design for time delay power systems, Energy Conversion and Management 49 (2) (2008) 193–204.
[6] Y. Rebours, D. Kirschen, M. Trotignon, S. Rossignol, A survey of frequency and voltage control ancillary services—Part I: Technical features, IEEE Transactions on Power Systems 22 (1) (2007) 350–357.
[7] N. Al-Musabi, Design of optimal variable structure controllers: applications to power system dynamics, Master's thesis, King Fahd University of Petroleum and Minerals, Dhahran, Saudi Arabia, 2004.
[8] J. Frunt, A. Jokic, W. Kling, J. Myrzik, P. van den Bosch, Provision of ancillary services for balance management in autonomous networks, in: Proceedings of the 5th International Conference on European Electricity Market, EEM 2008, 2008, pp. 1–6.
[9] B. Fardanesh, Future trends in power system control, IEEE Computer Applications in Power 15 (3) (2002) 24–31.
[10] P. Ibraheem, D. Kumar, Kothari, Recent philosophies of automatic generation control strategies in power systems, IEEE Transactions on Power Systems 20 (1) (2005) 246–357.
[11] H. Shayeghi, H. Shayanfar, A. Jalili, Load frequency control strategies: a state-of-the-art survey for the researcher, Energy Conversion and Management 50 (2) (2008) 344–353.
[12] I. Ngamroo, C. Taeratanachai, S. Dechanupaprittha, Y. Mitani, Enhancement of load frequency stabilization effect of superconducting magnetic energy storage by static synchronous series compensator based on Hoo control, Energy Conversion and Management 48 (4) (2006) 1302–1312.
[13] E. Cam, Application of fuzzy logic for load frequency control of hydro-electrical power plants, Energy Conversion and Management 48 (4) (2007) 1281–1288.
[14] H. Lee, J. Park, Y. Joo, Robust load-frequency control for uncertain nonlinear power systems: a fuzzy logic approach, Information Sciences 176 (23) (2006) 3520–3537.
[15] S. Pothiya, I. Ngamroo, S. Runggeratigul, P. Tantaswadi, Design of optimal fuzzy logic based pi controller using multiple tabu search algorithm for load frequency control, Control, Automation, and Systems 4 (2) (2006) 155–164.
[16] A. Hemeida, Wavelet neural network load frequency controller, Energy Conversion and Management 46 (9–10) (2005) 1613–1630.
[17] Y. Oysal, A.S. Yilmaz, E. Koklukaya, A dynamic wavelet network based load frequency control in power systems, International Journal of Electrical Power & Energy Systems 27 (1) (2005) 21–29.
[18] H. Shayeghi, H. Shayanfar, Application of ANN technique based on μ-synthesis to load frequency control of interconnected power system, International Journal of Electrical Power & Energy Systems 28 (7) (2006) 503–511.
[19] N. Atic, A. Feliachi, D. Rerkpreedapong, CPS1 and CPS2 compliant wedge-shaped model predictive load frequency control, in: Proceedings of the 2004 IEEE Power Engineering Society General Meeting, 2004, pp. 855–860.
[20] A. Venkat, I. Hiskens, J. Rawlings, S. Wright, Distributed output feedback MPC for power system control, in: Proceedings of the 45th IEEE Conference on Decision and Control, San Diego, USA, 2006.
[21] A. Demiroren, H. Zeynelgil, GA application to optimization of AGC in three-area power system after deregulation, Electrical Power and Energy Systems 29 (3) (2007) 230–240.
[22] C. Parisses, N. Asimopoulos, P. Fessas, Decentralized load-frequency control of a two-area power system via linear programming and optimization techniques, in: Proceedings of the 5th International Conference on Technology and Automation, Thessaloniki, Greece, 2005, pp. 204–209.
[23] S. Velusami, I. Chidambaram, Decentralized biased dual mode controllers for load frequency control of interconnected power systems considering GDB and GRC non-linearities, Energy Conversion and Management 48 (5) (2007) 1691–1702.

[24] L. Chang-Chien, J. Cheng, The online estimate of system parameters for adaptive tuning on automatic generation control, in: Proceedings of the International Conference on Intelligent Systems Applications to Power Systems, Niigata, Japan, 2007, pp. 1–6.
[25] S. Hosseini, A. Etemadi, Adaptive term neuro-fuzzy inference system based automatic generation control, Electric Power Systems Research 78 (7) (2008) 1230–1239.
[26] M. Zribi, M. Al-Rashed, M. Alrifai, Adaptive decentralized load frequency control of multi-area power systems, International Journal of Electrical Power & Energy Systems 27 (8) (2005) 575–583.
[27] M. Alrifai, Decentralized controllers for power system load frequency control, ICGST International Journal on Automatic Control and System Engineering 5 (2) (2005) 1–16.
[28] M. Yang, H. Lu, Sliding mode load-frequency controller design for dynamic stability enhancement of large-scale interconnected power systems, in: Proceedings of the IEEE International Symposium on Industrial Electronics, Bled, Slovenia, 1999, pp. 1316–1321.
[29] Y. Hsu, W. Chan, Optimal variable structure controller for the load-frequency control of interconnected hydrothermal power systems, Electrical Power and Energy Systems 6 (4) (1984) 221–229.
[30] Q. Ha, A fuzy sliding mode controller for power system load-frequency control, in: Proceedings of the Second International Conference on Knowledge-Based Intelligent Electronic Systems, 1998, pp. 149–154.
[31] F. Okafor, Variable structure unit vector control of electric power generation, African Journal of Science and Technology - Science and Engineering Series 1 (4) (2001) 78–86.
[32] Z. Al-Hamouz, H. Al-Duwaish, A new load frequency variable structure controller using genetic algorithms, Electric Power Systems Research 55 (1) (2000) 1–6.
[33] C. Edwards, S. Spurgeon, Sliding Mode Control: Theory and Applications, Taylor and Francis, 1998.
[34] S. Janardhanan, Multirate output feedback based discrete-time sliding mode control strategies, Ph.D. thesis, Indian Institute of Technology, Bombay, India, 2005.
[35] G. Monsees, Discrete-time sliding mode control, Ph.D. thesis, Delft University of Technology, Netherlands, 2002.
[36] M. Saaj, B. Bandyopadhyay, H. Unbehauen, A new algorithm for discrete-time sliding-mode control using fast output sampling feedback, IEEE Transactions on Industrial Electronics 49 (3) (2002) 518–523.
[37] V. Bandal, Power system stabilizer design based on multirate output feedback sliding mode control strategies, Ph.D. thesis, Indian Institute of Technology, Bombay, India, 2005.
[38] A. Ben-Israel, T. Greville, Generalized Inverses, Springer-Verlag, 2003.
[39] L. Han, M. Neumann, Handbook of Linear Algebra, Chapman & Hall/CRC, 2007, Ch. Inner Product Spaces, Orthogonal Projection, Least Squares, and Singular Value Decomposition.
[40] V. Utkin, Sliding Modes in Control Optimisation, Springer-Verlag, 1992.
[41] K. Vrdoljak, V. Tezak, N. Peric, A sliding surface design for robust load-frequency control in power systems, in: Proceedings of the Power Tech 2007, Lausanne, Switzerland, 2007, pp. 279–284, http://ewh.ieee.org/conf/powertech.
[42] S. Sarpturk, Y. Istefanopulos, O. Kaynak, On the stability of discrete time sliding mode control systems, IEEE Transactions on Automatic Control 32 (10) (1987) 930–932.
[43] K. Furuta, Sliding mode control of discrete system, System & Control Letters 14 (2) (1990) 145–152.
[44] W. Gao, Y. Wang, A. Homaifa, Discrete time variable structure control systems, IEEE Transactions on Industrial Electronics 42 (2) (1995) 117–122.
[45] A. Bartoszewicz, Discrete-time quasi-sliding mode control strategies, IEEE Transactions on Industrial Electronics 45 (4) (1998) 633–637.
[46] S. Spurgeon, Hyperplane design techniques for discrete-time variable structure control systems, International Journal on Control 55 (2) (1992) 445–456.
[47] T. Radosevic, K. Vrdoljak, N. Peric, Optimal sliding mode controller for power system's load-frequency control, in: Proceedings of the 43rd International Universities Power Engineering Conference, Padova, Italy, 2008, pp. 1–5.
[48] K. Vrdoljak, N. Peric, M. Mehmedovic, Optimal parameters for sliding mode based load-frequency control in power systems, in: Proceedings of the 10th International Workshop on Variable Structure Systems, Antalya, Turkey, 2008, pp. 331–336.
[49] D. Ashlock, Evolutionary Computation for Modeling and Optimization, Springer, 2004.
[50] S. Tripathy, R. Balasubramanian, P. Chandramohanan, Small rating capacitive energy storage for dynamic performance improvement of automatic generation control, Generation, Transmission and Distribution IEE Proceedings C 138 (1) (1991) 103–111.
[51] A. Demiroren, E. Yesil, Automatic generation control with fuzzy logic controllers in the power system including SMES units, Electrical Power and Energy Systems 26 (4) (2004) 291–305.
[52] M. Baric, I. Petrovic, N. Peric, Neural network based sliding mode controller for a class of linear systems with unmatched uncertainties, in: Proceedings of the IEEE 41st Conference on Decision and Control, CDC02, Las Vegas, Nevada, 2002, pp. 967–972.